Light-induced thermal hysteresis and high-spin low-spin domain formation evidenced by optical microscopy in a spin-crossover single crystal

Houcem Fourati,[1] Mamadou Ndiaye ⬤,[1] Mouhamadou Sy,[1,2] Smail Triki,[3] Guillaume Chastanet,[4]
Sébastien Pillet,[5] and Kamel Boukheddaden ⬤[1,*]

[1]*Université Paris-Saclay, UVSQ, CNRS, GEMAC, UMR 8635, 45 Avenue des Etats Unis. F78035 Versailles Cedex, France*
[2]*Département de Physique, Université Assane Seck de Ziguinchor, LCPM, BP 523, Ziguinchor, Senegal*
[3]*Université Brest, CNRS, CEMCA, 6 Avenue Victor Le Gorgeu, C.S. 93837-29238 Brest Cedex 3, France*
[4]*Institut de Chimie de la Matière Condenssée de Bordeaux, Universitsé de Bordeaux, 87 Av. Doc. A. Schweitzer, F-33608 Pessac, France*
[5]*Université de Lorraine, CRM2 UMR 7036 54000 Nancy, France*

The low-temperature photoinduced effects of the spin-crossover $[\{Fe(2\text{-pytrz})_2[Pd(CN)_4]\}].3H_2O$ single crystal have been investigated by means of a cryogenic optical microscopy technique down to 10 K from which the imaging and quantitative analysis of the spatiotemporal transformation are derived. The magnetic investigations revealed that this compound exhibits an incomplete spin transition between a full high-spin (HS) state at high temperature and an intermediate HS and low-spin (LS) state, where HS and LS species coexist, as a result of the existence of an elastic frustration at the molecular scale, most likely caused by the rigidity of the interconnected $[Pd(CN)_4]$ $[Fe(II)/Pd(II)]$ two-dimensional network. At low temperature (10 K), thanks to reverse light-induced excited spin-state trapping effect, we could switch the system from the intermediate HS-LS state to the fully photoinduced LS state by irradiating the sample in near-infrared region, revealed by photomagnetic and optical microscopy studies. Optical microscopy images showed monotonous and homogeneous transformation of the crystal color along this process, corresponding to a gradual change of the spin state under light. In contrast, the thermal relaxation in the dark of this photoinduced LS-LS state shows a transition to the intermediate HS-LS state at ∼90 K with domain formation, which is characteristic of a first-order transition at equilibrium. Interestingly, the same behavior is also obtained during the heating process of the reverse light-induced thermal hysteresis cycle with a heating branch almost unchanged, confirming that light does not act on this transition. It is then concluded that the transition from the full LS to the intermediate HS-LS transition is of first order and therefore the LS state reached by light is a hidden stable state of the system until ∼90 K. These experimental results are modeled using an adapted version of the electroelastic model including photoexcitation effects and solved by Monte Carlo method. Both thermal equilibrium and light-induced thermal hysteresis are reproduced, in fair qualitative agreement with the experimental data of photomagnetism and optical microscopy.

I. INTRODUCTION

Spin-crossover (SCO) solids are among the largest examples of molecular switchable solids [1–3] which are explored for future applications as optical memories, numerical displays, and sensors [4–6]. Most of SCO compounds are based on iron (II) complexes, surrounded, in particular, by nitrogen atoms in an octahedral symmetry [7]; however, other examples based on Co or Mn ions have been also reported in the literature [8,9]. Depending on the strength (weak or strong) of the ligand field acting on the metal center, two possible respective electronic states, namely, the high-spin (HS) state ($S = 2$) and low-spin (LS) state ($S = 0$), may emerge. In the solid state, SCO materials may switch between these two spin states by various external stimuli such as temperature, pressure, light [1,10,11], etc. The spin transition is accompanied by a large change of physical properties (magnetization, color, volume,

etc.) which can be monitored by several techniques such as Mössbauer spectroscopy, x-ray diffraction, optical absorption, Raman and infrared spectroscopies, optical microscopy (OM), calorimetry [12–27], etc.

The literature of SCO materials is very rich and shows several types of thermal behaviors for the HS fraction, n_{HS}, which constitutes the order parameter describing the spin transition. From this literature, we can classify the SCO materials according to their thermal behaviors which lead to identify (i) noncooperative SCO materials, that is the case where the HS fraction evolves gradually with temperature following a Boltzmann distribution, (ii) strong cooperative systems, exhibiting first-order transition accompanied with a large thermal hysteresis, and (iii) others undergoing incomplete or multistep transitions, where the thermal dependence of the HS fraction goes through plateau regions [28,29]. It is important to notice that in the case of incomplete spin transitions, the intermediate plateau trapped at low temperature, containing a mixture or an ordered structure of HS and LS species, could be the result of kinetic trapping during the cooling process. In contrast, in

*kamel.boukheddaden@uvsq.fr

the case of the multistep transitions, except the trivial case of the presence of intrinsic structurally inequivalent iron sites in the lattice, there are competing antagonist elastic interactions which produce an elastic frustration [30] in the system, which leads to the emergence of plateaus at the transition with spatially self-organized spin states.

From the theoretical point of view, many models are used to describe the spin-crossover phenomenon, among them the microscopic models [31–33] such as electroelastic model which takes into account the deformations of the lattice accompanying the spin transition. Indeed, the switching of the spin states creates local deformations which propagate in whole the lattice due at the same time to their interference and reflection at the open surface boundary of the system. This is at the origin of the long-range elastic interactions. A complete imaging of the SCO processes in various temperature and optical irradiation conditions has been provided by OM studies [34]. In particular, OM studies performed on individual SCO single crystals demonstrated that the sudden significant volume change at the transition in cooperative spin transition material can cause macroscopic cracking of the crystal [18]. In contrast, for the robust single crystals involving a half of the spin transition or other systems in which anisotropic lattice parameter variations take place at the transition, it was revealed a single-domain nucleation of the spatiotemporal dynamics of the spin transition [20–23,35,36].

A crucial feature of SCO materials relates with their photoinduced bistability, allows a new way of conversion between the LS and HS spin states, a phenomenon which is based on the light-induced excited spin-state trapping (LIESST) effect. This single molecular process confers to the solid materials new out of equilibrium properties which are still under study until now. The first mention of the LIESST effect was reported by Decurtins *et al.* [37,38] in 1984 on the prototype SCO complex $[Fe(ptz)_6](BF_4)_2$. As it is now well admitted, the direct-LIESST effect consists in the switching of LS molecules at very low temperature by usually green-light irradiation through a Franck-Condon process which results in the population of the HS state after nonadiabatic and nonradiative relaxation from the high-energy excited states [39,40]. During the phototransformation, the lattice distances increase gradually to reach the HS lattice spacing value. At the end, the generated photoinduced metastable HS state becomes very stable at low temperature, even after switching off the light and may survive in some cases several months at 10 K, when tunneling relaxation effect due to second-order spin-orbit coupling is weak. In contrast, increasing temperature (with light off) results in the disappearance of this metastable state which relaxes at relatively low temperature by thermal activation to the stable equilibrium LS state. Similarly, starting from the previous metastable HS state at low temperature (prepared by light or by flash cooling) and irradiating the sample with red light causes the reverse-LIESST effect [41] consisting in populating the LS state by light at low temperature. The quantum process of this phenomenon is quite similar to that of the direct-LIESST effect, although it involves different excited states and leads to lower quantum yield. These mechanisms and the resulting thermally activated tunneling processes that allow their thermal relaxation are quite well explained by the theory of nonadiabatic multiphonon relaxation [42] for single molecular processes, which was extended later for cooperative systems [43]. Since this discovery, many types of theoretical and experimental studies have been developed in this field of photoinduced phenomena, opening the way to the discovery of new out-of-equilibrium phase transitions, such as the light-induced thermal hysteresis (LITH), which consists in emerging thermal hysteresis at low temperature between the LS and the HS states under permanent irradiation. This effect was concomitantly observed in Bordeaux [44] and Versailles [45] groups. In Ref. [45], this effect was modeled and explained as resulting from the competition between a linear random single molecular photoexcitation process which populates the HS states and a thermally activated nonlinear cooperative relaxation, involving macroscopic energy barriers which nonlinearly depend on the fraction of the populated molecules. It is, however, worth to mention that these phenomena were evidenced by photomagnetic studies, although they were later on confirmed using photocrystallographic investigations too [46]. Nevertheless, the direct imaging of the LITH phenomenon on a unique single crystal is quite rare, although several OM studies were conducted to reveal the spatiotemporal aspects of the thermally induced spin transition in a single crystal and the dynamics of the interface propagation accompanying the crystal's transformation between the LS and the HS states [36,47]. More complex studies, based on the photothermal control of the interface motion inside the thermal hysteresis of a SCO single crystal, were also reported [23,34,40,48]. However, the direct observation of the LIESST effect by OM was reported only once in [40], while the reverse-LIESST effect was never visualized on a SCO single crystal. Therefore, we aim here to investigate the photoinduced effects by OM on a cooperative single crystal of the compound $[\{Fe(2\text{-pytrz})_2[Pd(CN)_4]\}].3H_2O$ [21] abbreviated here as **1** which undergoes a half-spin transition between the full HS state and an intermediate HS-LS state. In addition, previous photomagnetic studies, performed on a powder sample, reveled the existence of a strong reverse-LIESST effect in this material by irradiation with a red light, which allows its switching at low temperature from the plateau state to the LS state. In this work, we examine this LITH hysteresis from both photomagnetic and OM experiments which address complementary physical properties and compare their responses in the light of the obtained results. However, we will mainly focus on the OM data which provide valuable information about the spatiotemporal mechanism of the light-excitation and the light-induced instability. These experimental investigations are complemented with a theoretical analysis based on the use of an extended version of the electroelastic model to qualitatively reproduce the experimental results. The paper is organized as follows: Section II contains chemical synthesis, magnetic measurements, and the optical microscopy technique of **1**. In Sec. III, we present the experimental findings on the magnetic, photomagnetic investigations and photoinduced spin transition including LITH effect, obtained by OM and discuss the spatiotemporal features of these transformations. In Sec. IV, we present the theoretical investigations using the electroelastic model. In Sec. V, we conclude and outline some possible developments of this work.

II. EXPERIMENTAL DETAILS

A. Synthesis and structural properties of [{Fe(2-pytrz)$_2$[Pd(CN)$_4$]}].3H$_2$O (1)

The 4-(2-pyridyl)-1,2,4,4H-triazole (2-pytrz) was prepared using the procedure described in Ref. [49]. Single crystals of [{Fe(2-pytrz)$_2$[Pd(CN)$_4$]}].3H$_2$O (**1**) were prepared by slow diffusion, according to Ref. [21]. The asymmetric unit of **1** contains two independent Fe(II) ions, Fe1 and Fe2, located on two special positions (an inversion center for Fe1 and a twofold axis for Fe2), one [Pd(CN)$_4$]$^{2-}$ anion, two 2-pytrz molecules acting as terminal ligands, and three solvent water molecules, all located in general positions. The two iron centers (Fe1 and Fe2) are alternately linked by the [Pd(CN)$_4$]$^{2-}$ anions, acting with a tetrabridging coordination mode to form neutral two-dimensional (2D) coordination layers of chemical formula [Fe(2-pytrz)$_2$ Pd(CN)$_4$]. The latter stack along the [1 0 −1] direction to form a three-dimensional (3D) crystal packing. Detailed chemical synthesis, structural descriptions can be found in Ref. [21] for **1** and in Ref. [50] for the isostructural complex [{Fe(2-pytrz)$_2$[Pd(CN)$_4$]}].3H$_2$O, based on [Pt(CN)$_4$]$^{2-}$ anion.

B. Magnetic measurements

Magnetic and photomagnetic measurements of **1** were performed with a Quantum Design MPMS-XL-5 SQUID magnetometer in the 2–300 K temperature range with an applied magnetic field of 2 T on assembly of single crystals of compound **1** (with mass of 0.68 mg). The photomagnetic characterizations of compound were carried out using a set of photodiodes. Irradiation was carried out at 10 K several times using different wavelengths (i.e., 650, 830, and 980 nm) to determine the most efficient conditions to reach a strong photoconversion yield at photosaturation. Reverse-LIESST experiments were performed by irradiating the sample at 10 K in the plateau region with a 830-nm diode laser (6 mW cm^{-2}), until reaching the saturation of the LS state.

C. Optical microscopy

Before proceeding to the OM investigations, the first experimental step is the selection of a clean single crystal with the minimum number of visible defects on the surface. We have been able to select one single crystal of compound **1** which has the typical lengths of ∼160 μm. For the experimental investigations, we used a Nikon Eclipse LV100 microscope, equipped with an Oxford cryostat and a Dalsa Falcon 1.4M100 camera which can capture up to 100 images per second. The single crystal was placed into a sample cell, which is itself fixed to the cold finger of a helium-flow Oxford cryostat. For an efficient thermal control and to ensure a thermal homogeneity in the sample cell, we fixed the temperature scan rate at 0.5 K min^{-1} for all the OM experiments and we configured the camera to save 10 images per second to record the different investigations. In addition, the OM setup is adapted to include an optical fiber which is used to irradiate the single crystal for photoinduced investigations on single crystal such as LIESST, reverse-LIESST, LITH, or to the control of HS/LS elastic interface propagation [34,51].

From every saved image, we extract the optical density (OD), defined as

$$\mathrm{OD} = \log_{10}(I_{\mathrm{incident}}/I_{\mathrm{transmitted}}), \tag{1}$$

where I_{incident} corresponds to the bright field intensity while $I_{\mathrm{transmitted}}$ corresponds to the intensity of the transmitted light through the single crystal. The OD is the key parameter of the data analysis (recorded images). It relates directly to the HS fraction, n_{HS}, of the single crystal, corresponding to the fraction of metal ions in HS state, and which connects to the normalized local OD:

$$n_{\mathrm{HS}} = \frac{\mathrm{OD}(x, y) - \mathrm{OD}_{\mathrm{LS}}}{\mathrm{OD}_{\mathrm{HS}} - \mathrm{OD}_{\mathrm{LS}}}, \tag{2}$$

where $\mathrm{OD}_{\mathrm{HS}}$ and $\mathrm{OD}_{\mathrm{LS}}$ are, respectively, the OD values in the HS and LS states. Each image of the experimental OM data was split into three OD components: red, green, and blue, depending on the single-crystal thickness and color. From one compound to another, the signal quality (signal-to-noise ratio) would perhaps be better, either in the red, green, or the blue pixel. All the data are analyzed using MATLAB programs developed in the Versailles group [21,22,24].

III. RESULTS AND DISCUSSION

A. Magnetic and photomagnetic studies

The magnetic susceptibility ($\chi_M T$) for **1** was determined over the 2–300 K temperature range on a polycrystalline sample. The ($\chi_M T$) versus T plot (where T is the temperature) is displayed in Fig. 1(a). In the high-temperature region, the $\chi_M T$ value (3.22 cm^3 K mol^{-1}) is consistent with a HS ($S = 2$) configuration of the hexacoordinated Fe(II) ions. Upon cooling, $\chi_M T$ remains almost constant down to about 160 K, at which it abruptly decreases to about 1.80 cm^3 K mol^{-1}, indicating the presence of an incomplete sharp HS-to-LS SCO first-order phase transition. Below 160 K, the $\chi_M T$ product remains almost constant with a residual fraction of about 57% Fe(II) ions in the HS configuration. This $\chi_M T$ value is slightly higher than half of the high-temperature value 3.22 cm^3 K mol^{-1} because of the presence of a paramagnetic fraction of about 7%, probably arising from a small paramagnetic residue or a partially dehydrated phase [50]. At very low temperatures, the fraction of HS Fe(II) ions shows the usual zero-field-splitting (ZFS) effect, leading to a decrease of the $\chi_M T$ product to 1.25 cm^3 K mol^{-1}. The warming mode shows a slight thermal hysteresis because the spin transition temperatures ($T_{1/2}$) for the cooling ($T_{1/2}^{\mathrm{down}}$) and warming ($T_{1/2}^{\mathrm{up}}$) modes are 160 and 163.5 K, respectively [see the inset of Fig. 1(a))], for a temperature scan rate of 0.4 K min^{-1} [21].

At 10 K, irradiation of the HS-LS state in the near-IR region ($\lambda = 830$ nm, $P = 6$ mW) for 60 min [Fig. 1(a)] induces a decrease of the $\chi_M T$ product from 1.25 to almost 0 cm^3 K mol^{-1}, indicating the occurrence of the reverse-LIESST effect. The time dependence of the magnetic signal along the reverse-LIESST process is presented in Fig. 1(b). There, we see that $\chi_M T$ value decreases following a stretched experimental behavior with the presence of a long tail, attributed to the double effect of photoheating and absorption of light inside the sample powder which slow down the photoexcitation process. An interesting aspect of this transformation,
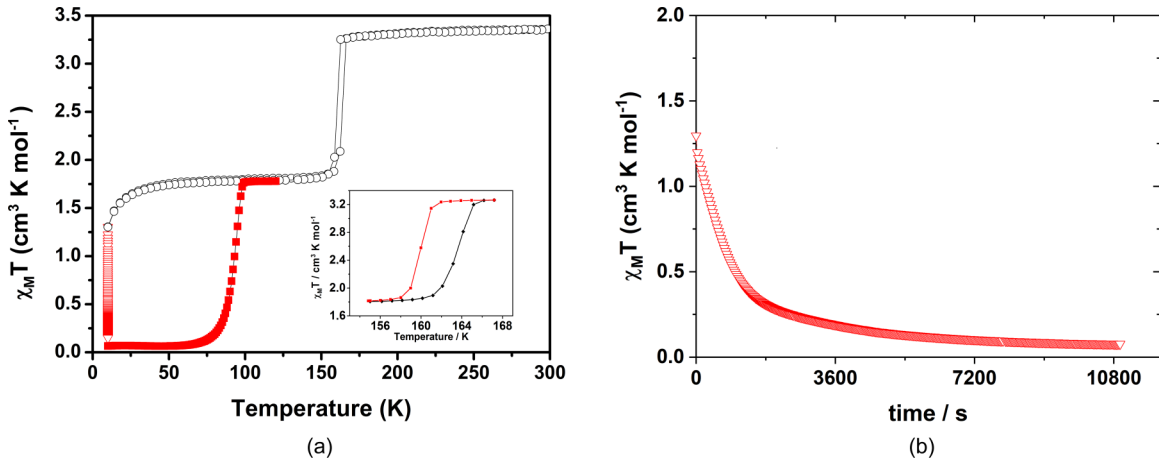
(a)   (b)

FIG. 1. Thermal evolution of the $\chi_M T$ product from high temperature to low temperature in the dark ($\circ$) and under red ($\triangledown$) light irradiation ($\lambda = 830$ nm, $P = 6$ mW) at $T = 10$ K, red ($\blacksquare$) is subsequent thermal relaxation in the dark with a temperature heating rate of 0.4 K min^{-1}. The inset figure represents a zoom of the thermal hysteresis loop indicating transition temperatures of 160 and 163.5 K, for cooling and heating, respectively [21].

which will be compared to optical microscopy data, is the long time of almost 2 h needed to switch the system from the intermediate state to the LS state.

Upon further warming, the $\chi_M T$ product increases to recover the value of the intermediate state at $T \simeq 100$ K [see Fig. 1(a)]. The derivative of the curve indicates a T (reverse-LIESST) value of 85 K. The stability of this photoexcited state has been checked through a detailed study on the analogous compound {Fe(2py-trz)[Pt(CN)$_4$]} in Ref. [50].

We summarize, in Fig. 2, the thermal dependence of the magnetic signal under permanent irradiation in reverse-LIESST regime. Here, a LITH appears as a result of a dynamical competition between the light excitation, which favors the metastable photoinduced state (the LS-LS state), and the temperature, which accelerates the sigmoidal relaxation of this photoinduced state towards the HS-LS state. The competition between these two processes (where the temporal evolution of the HS fraction follows a nonlinear trend) results
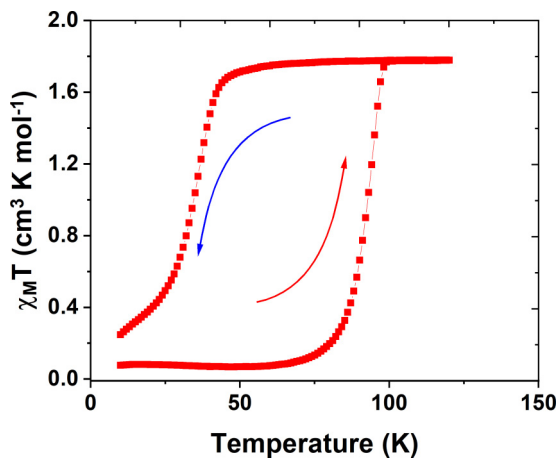
in a photoinduced thermal instability, which is accompanied by hysteretic behavior. That is the LITH loop depicted in Fig. 2, which reveals the existence of a nonequilibrium transition involving photoinduced and thermally induced states. Because of their dynamical character, usually the LITH loops are very sensitive to the temperature scan rate, leading to wide LITH loops when the temperature scan rate is slow enough. The absence of any influence of 830-nm irradiation on the thermal dependence of the LS−LS state upon heating (Fig. 2) and on its relaxation kinetics (Fig. 1) strengthens the argument that the heating branch of the reverse-LITH curve, located around $T \simeq 80$ K, describes the thermally induced spin transition of a hidden stable LS−LS state toward the LS−HS phase.

B. Optical microscopy investigations

Cryogenic OM technique is a powerful setup to visualize and investigate in real time the spatiotemporal aspects of spin transition in SCO single crystals. Based on the color change property during phase transition of SCO materials one can monitor the change and quantify the spin transition. As mentioned in the Introduction, a variety of SCO single crystals [14–25] present visible spatiotemporal aspects with well-defined elastic interfaces during their first-order phase transition between the high- and low-temperature phases. The thermoinduced spin transition between the full HS and the intermediate HS-LS states of single crystals of compound **1** were well investigated using OM in Ref. [21]. They undergo an incomplete spin transition between a full HS state and an intermediate HS-LS state with single-domain propagation, indicating the presence of elastic interactions between the SCO centers. In this study, we will focus on the low-temperature experiments using (OM) to follow the spatiotemporal aspects of the transitions under light. We will particularly investigate the system properties in the course of the reverse-LIESST and reverse-LITH regimes which showed particular behaviors in magnetic investigations, with the presence of hidden stable LS-LS state at low temperature. At this end the OM setup is

FIG. 2. Thermal evolution of the $\chi_M T$ product, under permanent red light irradiation ($\lambda = 830$ nm, $P = 6$ mW) in the reverse-LIESST regime on warming and cooling modes, leading to a reverse-LITH. Temperature scan rate was $r = 0.4$ K min^{-1}.
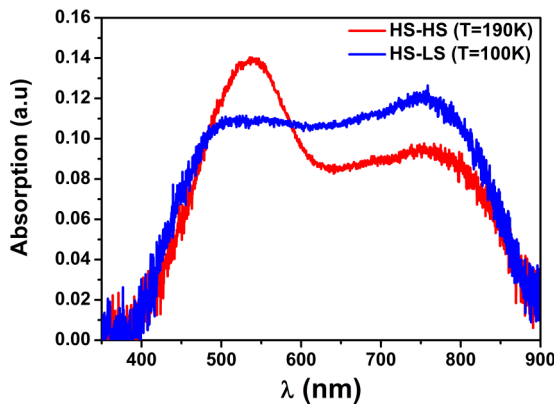
FIG. 3. The absorption spectra of compound **1** in the HS-HS state (red curve) at $T = 190$ K and in the HS-LS state (red curve) at $T = 100$ K, taken from the OM experiment.

adapted to include photoexcitation experiments injecting the light through the objective of the microscope using an optical fiber, allowing to irradiate the single crystal using the desired wavelength.

1. Absorption spectra

To confirm the results of the magnetic investigations of Fig. 1 which showed a sensitivity of the compound **1**, to red light irradiation, we measured by OM the absorption spectra on one single crystal in the visible region. Figure 3 illustrates the absorption bands of compound **1**, for the HS-HS and HS-LS states represented by red and blue curves, respectively. The obtained results are collected through the optical fiber connected to the microscope and to Ocean Optics Inc S2000 spectrometer. We can remark that the single crystal has a relatively higher absorption in the green region in the HS-HS state (red curve) with a band around $\lambda \simeq 540$ nm while it turns to near-infrared region ($\lambda \simeq 740$ nm) in the HS-LS state (blue curve). These results are in good agreement with the photomagnetic data presented in Fig. 1, which demonstrated an efficient photoinduced HS-LS to LS-LS conversion under 830-nm excitation.

2. Reverse-LIESST photoexcitation by OM

The results of the photomagnetic experiments provide converging evidence of the stability of the photoinduced LS-LS state at low temperature. In this section, we examine by OM the light-induced properties of a single crystal of compound **1**, using a photoexcitation wavelength $\lambda = 790$ nm with a power intensity $P = 0.11$ mW. We also add a red filter to the microscope in order to obtain clear images helping to better quantify the OD variation during the photoexcitation process. In practice, first we start by cooling the system in the dark until reaching $T = 10$ K, then the light is switched on to start the photoexcitation process. Following the average OD variation of each saved image during the photoexcitation process, we obtain Fig. 4(a) which shows the temporal evolution of the HS fraction, n_{HS}. Here, we see that the single crystal takes around 15 min to reach the LS-LS state from the intermediate HS-LS state, following a single exponential behavior, which
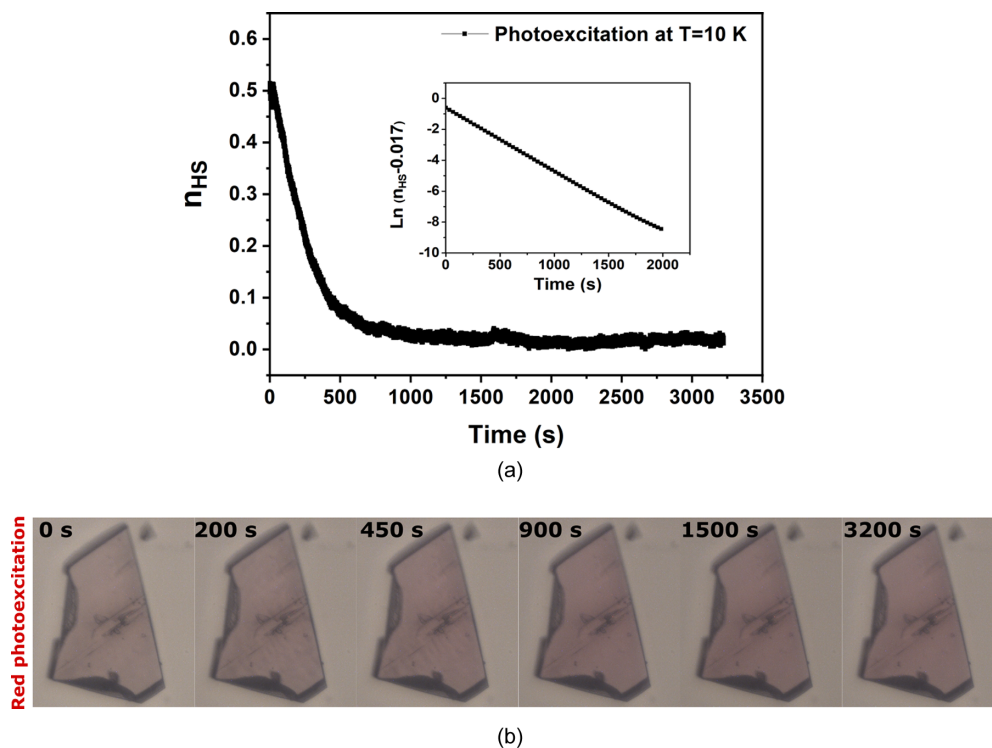

(a)

(b)

FIG. 4. (a) Time dependence of the HS fraction during the reverse-LIESST process between HS-LS and LS-LS states, derived from OM study. Excitation wavelength was $\lambda = 790$ nm, power intensity was $P = 0.11$ mW, and temperature was $T = 10$ K. (b) Selected snapshots of the single crystal at different times along the photoexcitation process showing the homogeneous character of the phototransformation (see Supplemental Material, video SM1 [52]). The photoexcitation process is complete within ~15 mn.
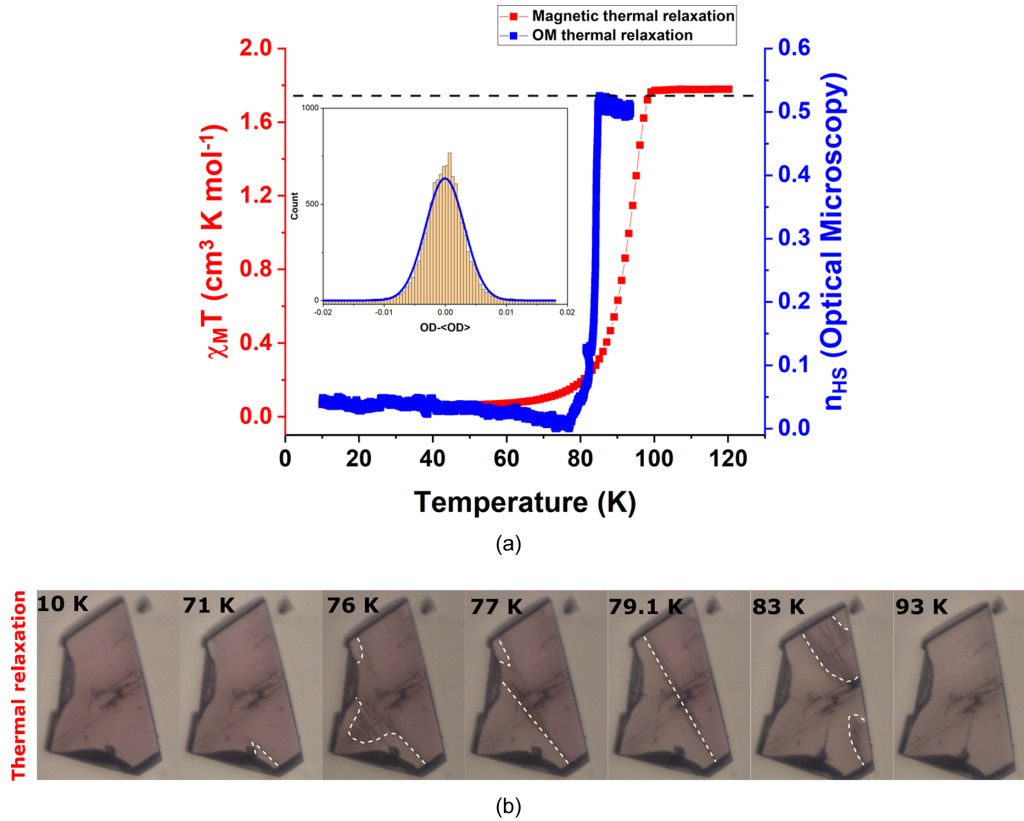
(a)

(b)

FIG. 5. (a) Temperature dependence of the magnetic signal (red curve) and OM response (blue curve) of compound **1** after reverse-LIESST photoexcitation during the thermal relaxation in the dark from LS-LS to HS-LS state. The discrepancy between the two curves is discussed in the text. Temperature rate was $r = 0.5$ K min^{-1} for OM and $r = 0.4$ K min^{-1} for magnetic experiment. Inset: histogram of the fluctuations of the OD around its mean value calculated for the LS and the intermediate HS-LS states and its Gaussian fitting. A standard deviation of 0.009 is obtained. (b) Selected snapshots of the single crystal of compound **1** collected from OM during the heating process showing a nucleation and growth process (see Supplemental Material, video SM2 [52]). Dashed white lines indicate the front interface between the HS-LS and LS-LS phases.

is typical of noncooperative character of this transition. This means that the LS fraction, $n_{LS} = 1 - n_{HS}$, follows the simple evolution law $dn_{LS}/dt = \sigma I n_{LS}$, where I is the intensity of the light irradiation and σ is a coefficient accounting for the quantum efficiency of the process and absorption of light through the sample. σ is assumed to be independent of n_{LS}, and the process is considered as isothermal. To confirm this trend we check that the logarithm of n_{HS} shows linear behavior with time [see inset of Fig. 4(a)], where the slope corresponds to the inverse of time required to transform the system from HS-LS to LS-LS evaluated here to $\simeq 15$ min. This switching time is quite short compared to that of photomagnetic studies, which is evaluated to $\simeq 30$ min [50]. Figure 4(b) displays some snapshots of the single crystal during the photoexcitation process showing a homogeneous transformation without the presence of any defined interface (see Supplemental Material, movie SM1 [52]).

3. Thermal relaxation in the dark and domain formation

From the photoinduced LS-LS state, at $T = 10$ K, we now heat the single crystal **1** in the dark, with a temperature heating rate of 0.4 K/min in order to measure its "thermal relaxation" to the HS-LS intermediate phase and to observe its spatiotem-

poral transformation. Here also the analysis is based on the OD variation during the heating in the dark, collected from the saved images. We represent in Fig. 5(a) (blue curve) the temperature dependence of the HS fraction, n_{HS}, obtained from the analysis of the OM images. The OM data are compared to the magnetic response (red curve) indicating significant differences. Indeed, the magnetic thermal relaxation reveals that the transformation starts at $T \simeq 70$ K and finishes around $T \simeq 100$ K. The starting temperature is very close to that of OM on single crystal, in contrast the transition is completed at $T = 85$ K in OM experiment. This gap can be attributed to the fact that magnetic experiments result in the statistical average of distributed transition temperatures of a large number of microcrystals with different shapes and sizes, whereas OM data relate to one single crystal's behavior. In addition, the temperature variation rate is slower for magnetic investigations which can affect also the kinetics of the transformation. Overall, all these aspects converge for obtaining sharper transitions in OM compared to magnetic investigations. Let us now discuss the spatiotemporal character of this thermal relaxation process. OM clearly indicates that the transformation process from LS-LS to HS-LS takes place with a nucleation and growth process as represented in Fig. 5(b) and in the Supplemental Material, movie SM2 [52]. We can also remark the

very slow character of the transition which starts at $T \simeq 71$ K and finishes at $T \simeq 85$ K. The snapshots of Fig. 5(b) illustrate an interface highlighted by dashed white lines, which has a diffusive and slow character compared to the results of the thermoinduced transition studied in Ref. [21] on the same compound. Indeed, a rough evaluation of the average interface velocity leads to $v \simeq 4.6$ μm/min which is almost 40 times smaller than the usual measured velocities of 3–5 μm/s in SCO materials at the thermal transition. This slow and diffusive character of the interface propagation during the transition is attributed to the difference in temperature. This 71–85 K range is lower than the HS-LS to HS thermal transition which takes place usually, for this compound, around 150–160 K in our similar OM experiments on single crystals. Indeed, the electroelastic energy barrier (elastic stresses) which faces to the propagation and the spread of the front interface can be considered, in a first approximation, as more or less the same for the LITH and thermal equilibrium hysteretic transitions. This claim is based on the fact that the elastic energy barrier depends on the lattice parameter misfit as well as on the interface length, although the elastic constants may depend on temperature. As demonstrated in Ref. [36], the velocity of the interface for the equilibrium thermal hysteresis can be written as $v = A[(\frac{1}{r}) \exp{(-\beta U_{HL})} - r \, \exp{(-\beta U_{LH})}]$, where r is a constant relating to the degeneracy ratio between the HS and the LS states and U_{HL} (respectively U_{LH}) are the respective energy barriers that the system must overcome to switch from LS to HS (respectively HS to LS) and $\beta = \frac{1}{k_B T}$ (T temperature). Then, the interface velocity follows an Arrhenius dynamics, which strongly depends on temperature. In fact, the temperature effect on the interface velocity already exists in the velocities of the heating and cooling branches of the equilibrium thermal hysteresis, while generally (but not systematically) the velocity of the interface is higher for the heating branch process than for the cooling in clean single crystals. In the present system, the slowing down of the interface velocity in the LITH region (around 90 K) compared to that of thermal equilibrium (around 160 K) is attributed to the combination of the significant temperature differences as well as the presence of defects and cracks generated by the several thermal cycling under light. This observation of interface propagation is characteristic of real first-order phase transition, showing the coexistence of two phases, thus confirming the thermodynamic stability of the LS-LS hidden state.

4. Reverse light-induced thermal hysteresis by OM: Selective domain formation

In this section, we aim to investigate the single-crystal properties under permanent irradiation. Our objective here is to produce the photoinduced thermal instability of the lattice through the reverse-LITH phenomenon. At this stage, we should mention that due to the different types of thermoinduced and photoinduced experiments and the stress generated by volume variation accompanying the spin transition, some irreversible cracks appeared on the single crystal. Despite of this, we should mention that this crystal seemed to be very robust comparing to previous materials [15,19], which were completely destroyed along the cooling process, thus preventing their complete study.

The same light source, of photoexcitation, is used for this reverse-LITH experiment ($\lambda = 790$ nm, $P = 0.11$ mW): the process consists on a cooling and heating the crystal under permanent irradiation. The experiment is started at $T = 100$ K, where the system is in the intermediate HS-LS state, the cooling and heating rate temperature is now $r = 0.5$ K min^{-1}. The analysis of the spatially averaged OD of the saved images is represented in Fig. 6(a) (blue curve), where we plotted the extracted HS fraction as a function of temperature for the cooling and heating processes. The snapshots of the all transformations, corresponding to different temperatures recorded along the thermal cycling, are given in Fig. 6(b) and in the Supplemental Material, movies SM3 and SM4 [52]. When cooling the system under red light, from 100 to 10 K, the crystal switches from the intermediate HS-LS state to the LS-LS state at $T \simeq 25$ K. This transformation cannot be realized without light irradiation as it is represented in Fig. 1. The switching of the system to the LS state is clearly due to the effect of the reverse-LIESST process which allows to populate the LS state. The efficiency of this optical process becomes stronger as the temperature is decreased, and so the observed switching temperature $T \simeq 25$ K crucially depends on the used intensity of light and on the temperature scan rate. Moreover, the analysis of the crystal snapshots [Fig. 6(b) and Supplemental Material, SM3 [52]] along the cooling process indicates that the transformation between the intermediate HS-LS and LS-LS states takes place in the homogeneous way, i.e., without any remarkable macroscopic single-domain nucleation. In contrast, one can observe in the snapshots of Fig. 6(b) and Supplemental Material, movie SM3 [52], at the corresponding temperature $T = 22$ K, the emergence of a spatial self-organization of the spin state, which manifests through the appearance of multiple dark domains in the single crystal. This self-organized structure, which shows dark stringlike lines observed at 22 K separating light regions of the crystal, is attributed to the competition between the effect of the light favoring the LS state which in turn absorbs more efficiently the red wavelength, thus heating the crystal and then favoring the HS-LS state, and temperature in a nonlinear way due to different optical absorption of the LS and HS phases, which causes their different photoheating, creating a self-organization of thermal gradients which are accompanied with mechanical stresses inside the crystal. This type of feedback is attributed to the complex spin-state structure which minimizes the strain effects caused by the antagonist roles of light and temperature in the vicinity of the thermal hysteresis [Fig. 6(a), blue curve]. It is worth noticing that these behaviors are linked to a theoretical predictive work [53], in which we found that self-organized spin-state structures can emerge from the competition between light and temperature in the vicinity of a thermal hysteresis. On the other hand, previous experimental studies [17,54,55] on light-induced self-organization of the spin states, performed by Laue neutron diffraction (on single crystal) and photomagnetic (on powder material) investigations suggested the occurrence of a light-induced phase separation in the LITH regime, but the latter was not imaged. The interpretation of these data was performed using a spatiotemporal version of the Ising-type model [56].
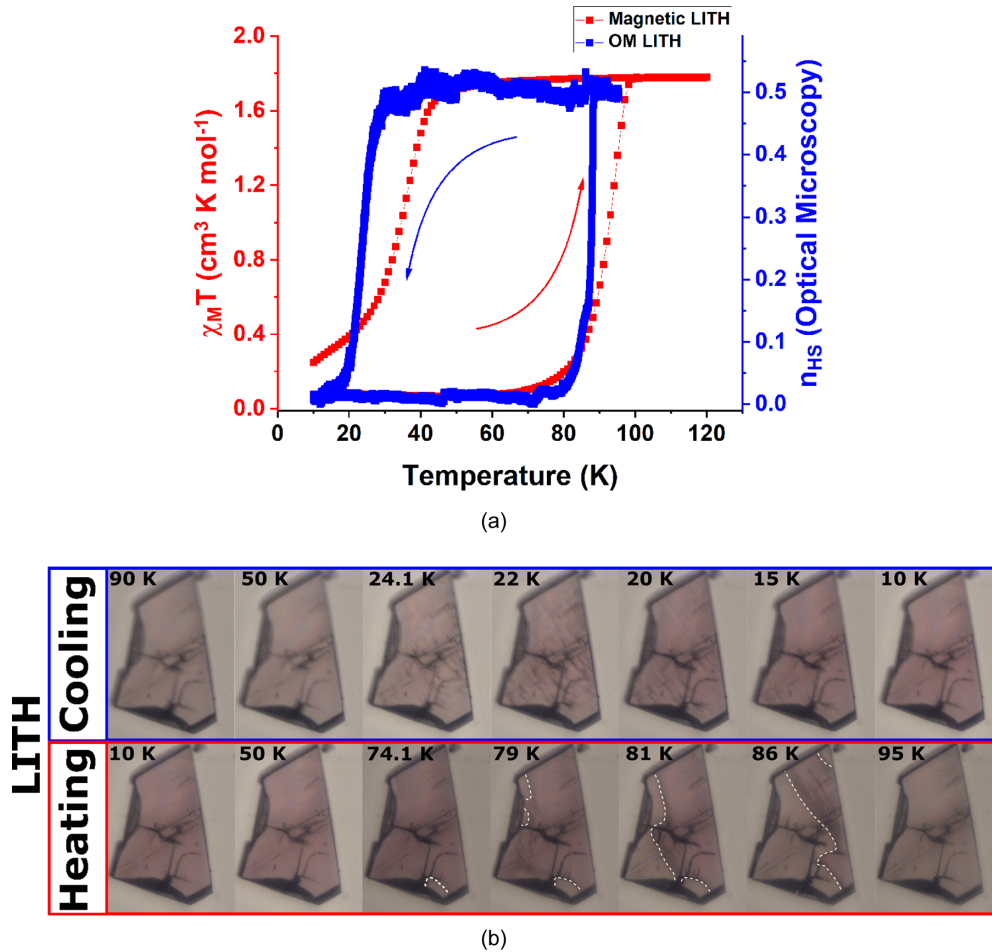
(a)

(b)

FIG. 6. (a) Temperature dependence of the magnetic (red curve) and OM (blue curve) responses of compound **1** during the reverse-LITH process between HS-LS and LS-LS states on cooling and heating processes. For OM: excitation wavelength was $\lambda = 790$ nm, power intensity was $P = 0.11$ mW, and temperature rate was $r = 0.5$ K min^{-1}. For magnetic experiment: excitation wavelength was $\lambda = 830$ nm, power intensity was $P = 6$ mW, and temperature rate was $r = 0.4$ K min^{-1}. The blue and red arrows indicate the cooling and heating processes, respectively. (b) Selected snapshots of the single crystal of compound **1** collected from OM during the cooling and heating processes, showing the homogeneous transformation on cooling (no domains) and the domain growth process on heating (see videos SM3 and SM4 in the Supplemental Material [52]). The dashed white lines on heating indicate the front interface between HS-LS and LS-LS phases.

On cooling, the HS fraction, corresponding to OM data of Fig. 6(a), starts to change from $T \simeq 29$ K, and reaches the LS state at $T \simeq 20$ K which then requires 18 min for the used temperature scan rate of 0.5 K/min. This switching time is very consistent with the 15 min found for the isothermal photoexcitation at 10 K, reported in Fig. 4(a), which indicates that we are facing to the same physical mechanism in both experiments. The magnetic response [Fig. 6(a), red curve] represented on the same graph, shows that transition on cooling starts at $T \simeq 45$ K almost 25 K before that of OM. This difference is due to several points: (i) the photoheating effects are stronger (more efficient) in the case of single-crystal study (OM) which maintains the crystal in the plateau region, (ii) the OM and photomagnetic experiments have been performed on different samples, viz., single crystals and microcrystalline powder, respectively, and (iii) the power intensity (6 mw) used in magnetic studies was higher than those utilized in OM, although in magnetic experiments significant light absorption must be accounted due to the millimetric thickness of the powder sample. Overall, the three effects contribute

to shift downwards the switching temperature of OM compared to that of magnetism. For the heating branch, where the system converts from the LS-LS state to the intermediate HS-LS state, one can observe a clear nucleation and propagation process during the transition very similar to that of the thermal relaxation in the dark of Fig. 5(b). Here, the transformation starts to nucleate at $T \simeq 74$ K and completes at $T \simeq 90$ K. Compared to the OM thermal relaxation in the dark of the Fig. 5, the present transition appears very similar since the temperature interval of the transition is 16 K while it was 14 K in Fig. 5. Thus, the reverse-LIESST process does not seem to have any effect on this transition, which clearly enforces the idea that this transition is a thermodynamic one, in the sense that it involves two equilibrium thermodynamic phases. On the other hand, the domain formation of this branch confirms the true first-order character of this phase transition and the stability of the LS-LS state. The less sharper magnetic branch on heating [red curve of Fig. 6(a)], starts almost at the same temperature, $T \simeq 72$ K, and reaches the HS-LS state at $T \simeq 100$ K. This gap is also

attributed to the difference between powder and single-crystal responses.

IV. THEORETICAL DESCRIPTION

A. Model

To model the incomplete spin transition with an intermediate HS-LS phase (with ordered pattern of HS and LS species) and the reverse-LITH process described in the previous section for the crystal **1**, we use the electroelastic model [57] which describes the spin transition phenomenon in 2D square lattices, that we are extending to two inequivalent sublattices, denoted $L1$ and $L2$. In this model, each SCO molecule representing a lattice site is associated with a fictitious spin state $S_i = \pm 1$, where $S_i = +1$ corresponds to the HS state and $S_i = -1$ to the LS state. To account for the molecular volume change during the spin transition, all the interactions between the nearest- and next-nearest neighbor sites may be considered through springs lattice whose elastic constants and the equilibrium distances depend on the spin states of the connected sites. The total Hamiltonian of a 2D system involving two sublattices is given by [57]

$$
\begin{aligned}
H &= \sum_{i \in L1} \frac{(\Delta_{L1} - k_B T \ \ln g) S_i}{2} + \sum_{i \in L2} \frac{(\Delta_{L2} - k_B T \ \ln g) S_i}{2} \\
&\quad + \frac{A}{2} \sum_{i \in L1, j \in L2} \left[r_{ij} - R_0 \left(S_i^{L1}, S_j^{L2} \right) \right]^2 \\
&\quad + \frac{B}{2} \sum_{\{i,k\} \in L1} \left[r_{ik} - R_0' \left(S_i^{L1}, S_k^{L1} \right) \right]^2 \\
&\quad + \frac{B}{2} \sum_{\{i,k\} \in L2} \left[r_{ik} - R_0' \left(S_i^{L2}, S_k^{L2} \right) \right]^2 .
\end{aligned} \tag{3}
$$

The first two terms of Eq. (3) are the energy gaps separating the LS and HS states of $L1$ and $L2$ isolated centers. They contain the energy contribution Δ_{L1} or Δ_{L2} arising from the difference of ligand field energies in the HS and LS states, and the entropic contribution $k_B \ln g$ resulting from the electrovibrational degeneracy ratio $g = \frac{g_{HS}}{g_{LS}}$, between the HS and LS states, which is assumed here as the same for both sites $L1$ and $L2$. The third term of the Hamiltonian (3) is the elastic energy contribution between the nearest-neighbor (NN) sites which belong to $L1$ and $L2$ lattices by construction. The fourth and the fifth terms are the next-nearest-neighbor (NNN) elastic energies which involve diagonal sites which naturally belong to the same sublattice, due to the checkerboard structure of the lattice.

$R_0(S_i, S_j)$, where S ($= S^{L1}$ or S^{L2}) is the NN equilibrium bond length between the nodes i and j depending on the bond type; $R_0(+1, +1) = R_0^{HH}$, $R_0(-1, -1) = R_0^{LL}$, and $R_0(+1, -1) = R_0(-1, +1) = R_0^{HL}$, where R_0^{HH}, R_0^{LL}, and R_0^{HL} are the respective equilibrium distances between nn HS-HS, LS-LS, and HS-LS sites. Thus, for the sake of simplicity, we consider here that the equilibrium distances between two HS-HS, HS-LS, or LS-LS sites are the same for sublattices $L1$ and $L2$. Whatever the considered sublattice, the expression of

$R_0(S_i, S_j)$ can be written under the following form:

$$
R_0(S_i, S_j) = R_0^{HL} + \frac{\delta_R}{4} (S_i + S_j), \tag{4}
$$

where $\delta_R = R_0^{HH} - R_0^{LL}$ is the lattice misfit between the HS and LS phases. For the sake of simplicity, the NNN equilibrium bond length $R_0'(S_i, S_j)$ is set equal to the NN equilibrium bond length multiplied by $\sqrt{2}$, $R_0'(S_i, S_k) = \sqrt{2} R_0(S_i, S_j)$ on the square lattice.

B. Resolution method

Hamiltonian (3) cannot be solved analytically due to its complex structure which mixes spin and distortion degrees of freedom, although a mean-field-like method [57] was recently developed for the case of one sublattice system, based on a homogeneous treatment of the lattice bond length, to speed up the simulations. However, its extension to the two-sublattice case faces serious problems, that make it an issue in itself. Therefore, the present Hamiltonian will be solved by Monte Carlo simulations, realized on both lattice and spin-state variables.

The study of the thermodynamic properties of the two-sublattice electroelastic 2D model (3) is performed on the 2D square lattice of size $N \times N = 30 \times 30$, with free boundary conditions. Each site interacts with its nearest neighbors (NN) and next-nearest neighbors (NNN) with respective elastic constants A and B and it feels the local ligand-field energy Δ_{L1} or Δ_{L2} according to which sublattice it belongs. The simulations are alternatively executed on spin and position variables in a two-step strategy. The Metropolis algorithm is considered for the spins and lattice positions update procedure (sites displacements). The choice of Metropolis dynamics is done here for practical considerations. Indeed, usually Arrhenius-type dynamics is more suitable for SCO systems particularly for spin models which do not account for vibronic intramolecular energy barriers [58,59], an aspect that has been already discussed in [60]. Thus, when using dynamical Ising models for SCO, an extra-energy barrier is introduced in the transition rates (keeping the detailed balance unchanged) to compensate the absence of the intramolecular energy barrier in the Hamiltonian. Naturally, when we deal with isothermal relaxation curves of the metastable HS fraction, the choice of the transition rate (Arrhenius, Metropolis, Glauber, etc.) is important and directly affects the system's trajectory in its phase space, causing different shapes for the relaxation curves: sigmoidal, stretched exponential, etc. Here, we use an elastic model to determine the equilibrium hysteresis and the LITH cycles. While for the former, the results are independent on the chosen transition rate (for the same detailed balance), in the latter, where the hysteresis is formed of a successive "nonequilibrium stationary states" will depend on the type of the chosen dynamics. For electroelastic or mechanoelastic or elastic models in general, flipping a spin state results in an elastic barrier which is usually (when the elastic constants are well chosen) sufficient to locally stabilize the HS structure at low temperature, as in the case of the photoexcitation process [61]. It is then not necessary to add an extra intramolecular energy barrier or to consider an Arrhenius dynamics, which considerably slows down the kinetic processes, and generate

strong metastable states, from which it is hard to escape. The stochastic algorithm is performed in the following way: for a site (i, j) randomly selected, with spin $S_{ij} = \pm 1$ and position r_{ij}, a new spin value S'_{ij} (such that $S_{ij} \rightarrow S'_{ij} = -S_{ij}$) is set without position change. This spin change is accepted or rejected by the usual Metropolis criterion. Whatever the result (acceptance or rejection), the whole lattice is relaxed mechanically by a slight motion of nodes (selected randomly) with a quantity $\delta u = 0.03$ (in any direction: $u = x, y$) which is much smaller than the distance between the spin states ($R_0^{LL} = 1.0$). The lattice relaxation is also performed following a Monte Carlo technique at fixed spin configuration. The procedure of the lattice relaxation is once repeated for each spin flip. Afterwards, a different spin site will be selected randomly and so on, etc. Once all nodes of the lattice are visited for the spin change, we define such step as the unit of the Monte Carlo step and denoted "MCS." Physical quantities of interest are calculated in the steady state with $N_S = 10^4$ MC steps per site for the spin-flip dynamics and for each spin-flip attempt, all SCO unit displacements are once attempted (one Monte Carlo cycle). About $N_E = 10^4$ MC steps per site are considered for reaching the thermal equilibrium in the spin-flip dynamics and then discarded from the averaging procedure. Three to five independent runs are performed on each MC process for thermal properties studies, in view to get smooth data. The lattice fictitious magnetization is calculated as follows:

$$m = \langle S \rangle = \frac{1}{N} \sum_{i=1}^{N} S_i. \qquad (5)$$

The latter connects to the HS fraction, n_{HS}, through the simple relation

$$n_{HS} = \frac{1 + \langle S \rangle}{2} = \frac{1 + m}{2}. \qquad (6)$$

C. Incomplete thermal spin transition and need of elastic frustration

The thermal properties of the system are determined by first cooling down from the HS state at 200 K to 1 K and then by warming up to the HS state at 200 K, with 1 K increments. The used model parameter values are as follows: $\Delta_{L1} = 200$ K and $\Delta_{L2} = 450$ K for the ligand field energies of the sites $L1$ and $L2$, $g = 150$ ($\ln g = 5$) for the degeneracy ratio leading to a transition temperature in case of weak elastic interactions or independent sublattices $T_{eq}^{L1,0} = \frac{\Delta_{L1}}{k_B \ln g} = 40$ K and $T_{eq}^{L2,0} = \frac{\Delta_{L2}}{k_B \ln g} = 90$ K. The values of the NN equilibrium bond lengths are taken equal to $R_0^{HH} = 1.2$ nm ($R_0^{LL} = 1.0$ nm) between two HS (LS) sites and $R_0^{HL} = \frac{R_0^{HH} + R_0^{LL}}{2} = 1.1$ nm between HS and LS sites. The NN elastic constant value is taken as $A = 10^4$ K nm^{-2} and that of NNN sites is $B = 10^3$ K nm^{-2}. When the elastic interactions are negligible compared to the ligand field energies, a plateau of a width $\Delta T^0 = T_{eq}^{L2,0} - T_{eq}^{L1,0} \simeq 50$ K preexists as a result of the inequivalence of the sites $L1$ and $L2$, as depicted in Fig. 7. However, by inserting the elastic interactions (nonzero elastic constants) in the system, the lower transition temperature T_{eq}^{L1} shifts upwards, while the higher transition temperature T_{eq}^{L2} shifts downwards, which results in the contraction of the plateau's width.
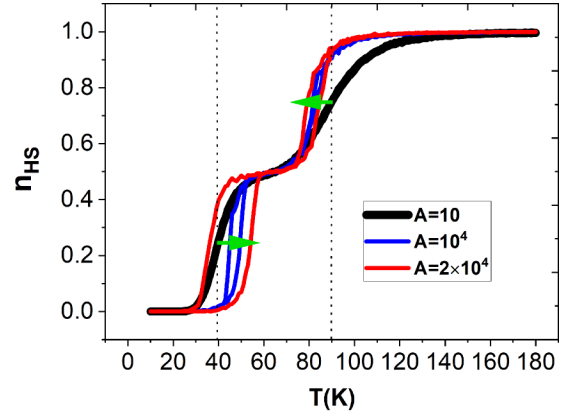

FIG. 7. Thermal dependence of the HS fraction, n_{HS}, for zero and nonzero elastic constants showing a shrinking of the plateau due to the increase of T_{eq}^{L1} upwards and the decrease of T_{eq}^{L2} downwards indicated by the green arrows. The parameter values are $\Delta_{L1} = 200$ K, $\Delta_{L2} = 450$ K, $\ln g = 5$, $A = 10^4$ K nm^{-2} (blue curve), $A = 2 \times 10^4$ K nm^{-2} (red curve), and $A = 10$ K nm^{-2} (black curve) and $B = 10^3$ K nm^{-2} for all curves.

Thus, to achieve the incomplete spin transition as observed in the experiment, another ingredient is necessary. This ingredient is the elastic frustration which is put here in the intermediate phase along the diagonal NNN sites. For that, we follow the idea we introduced in Refs. [62,63] based on the introduction of a kind of a geometric frustration between NNN HS-LS and LS-LS sites while the HS-HS configurations are taken free from elastic frustration.

The elastic frustration is considered here in the equilibrium NNN bond lengths which are now written as follows:

$$d_{NNN}(S_i = 1, S_k = 1) = \sqrt{2} R_0^{HH},$$
$$d_{NNN}(S_i = \pm 1, S_k = \mp 1) = \sqrt{2} \left[R_0^{HL} + \xi \delta R_0 \right],$$
$$d_{NNN}(S_i = -1, S_k = -1) = \sqrt{2} \left[R_0^{LL} + \frac{1}{2} \xi \delta R_0 \right], \qquad (7)$$

where ξ is the rate of elastic frustration. It is important to notice here that the NN equilibrium distances are still given by the expressions of Eq. (4), which means that $R_{NN}^{HH} = R_0^{HH}$, $R_{NN}^{HL} = R_0^{HL}$, and $R_{NN}^{LL} = R_0^{LL}$, which creates an antagonism between the NN and NNN equilibrium distances. As indicated in Eq. (7), the HS-LS configuration is more frustrated than the LS-LS.

The stabilization of the intermediate plateau at $n_{HS} = 0.5$ in this cooperative system is made possible thanks to combined effects of elastic frustration and vanishing of thermal fluctuations at low temperature. On the other hand, the increase of the elastic constant A increases the energy barrier between the intermediate (HS-LS) and the fundamental (LS) states, which then precludes the thermal conversion between these two states. Figure 8(a) shows clearly that the HS fraction switches in a first-order fashion between the HS state and the intermediate ordered HS-LS phase around $T \simeq 80$ K. The metastable nature of this latter phase is evidenced in Fig. 8(b), where we performed the MC simulations by starting from the LS state, for $A = 10\,000$ K nm^{-2}. Here, a clear hidden LS state appeared, which is stable until $T \simeq 50$ K, from which
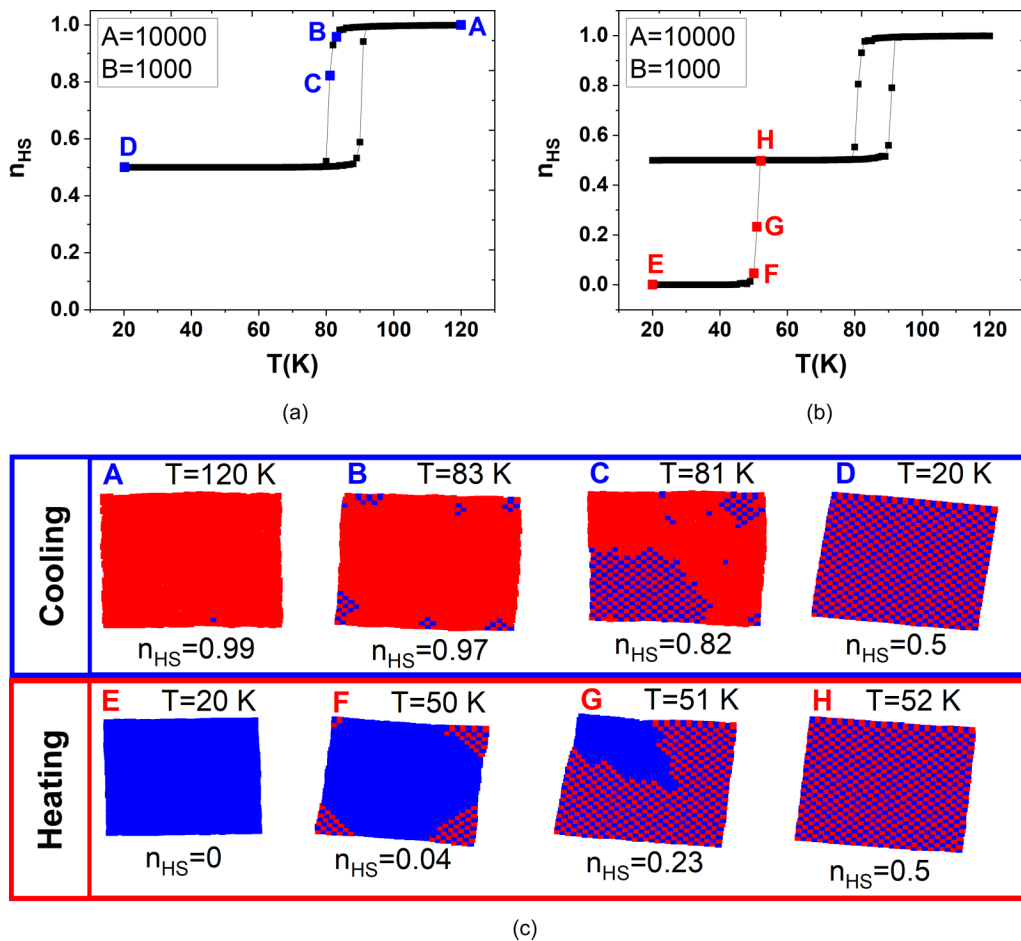
FIG. 8. Thermal dependence of the HS fraction, n_{HS}, for MC simulations starting from (a) the HS state, showing a half-hysteretic spin transition with a large plateau; (b) for simulation starting from the LS state showing double-step transition with the presence of a hidden stable LS state which remains stable until $T \sim 50$ K. (c) Selected snapshots highlighting the spatiotemporal behavior of the HS and LS sites, associated with thermal transition curves for points A, B, C, D on cooling for (a) and E, F, G, H on heating for (b) showing macroscopic domains growing from the corners and self-organization of the spin states. Blue and red squares correspond to LS and HS sites, respectively. The parameter values are the same as those of Fig. 7, except for $A = 10^4$ K nm^{-2} and $B = 10^3$ K nm^{-2}.

the system switches to the intermediate HS-LS state, and then later to the HS state at $T = 90$ K, thus leading to a double-step transition. The snapshots of the spatial organization of the spin states corresponding to the cooling process of Fig. 8(a) is shown in the top A–D points of Fig. 8(c), where we see that the first-order character of this transition induces the appearance of macroscopic domains of the intermediate state starting from all corners and propagating towards the center of the lattice. This transformation is also accompanied with the distortion and contraction of the lattice, which stops in the ordered state (D). On heating from the LS state (E–H), a similar behavior of macroscopic domain growth, characteristic of first-order transition, takes place between the LS and the intermediate HS-LS state in the first instance, followed by the second transition between the HS-LS and the HS states with the same mechanism except that now the lattice volume expands along the transformation.

D. Photoinduced processes

In this section, we analyze the effect of light on the intermediate plateau found in Fig. 8. In particular, we will focus on

the case of reverse-LIESST effect in order to understand the effect of light on the organization of the highly ordered plateau and its light-induced switching to the LS state. For more understanding of the photoinduced processes and after finding the best parameter of the model that reproduce qualitatively the experimental behavior, we include the photoexcitation process in the Monte Carlo procedure [60,61,64,65] through the introduction of a bias in the detailed balance where we consider an energy barrier E_0 between the HS and LS states which represent the threshold to switch from one state to another. The total transition rate must contain two terms, one related to the thermally induced spin transition, and a second accounting for the contribution of light. Since the two processes are uncorrelated, we can write

$$W^{\text{tot}}(S_i \rightarrow -S_i) = W^{\text{ther}}(S_i \rightarrow -S_i) + W^{\text{opt}}(S_i \rightarrow -S_i),$$
(8)

where $W^{\text{ther}}(S_i \rightarrow -S_i)$ is the usual Metropolis rate transition, whose expression is given by $W^{\text{ther}}(S_i \rightarrow -S_i) = \min\{1, \exp[-E(-S_i) + E(S_i)]\}$. The optical transition probability $W^{\text{opt}}(S_i \rightarrow -S_i)$ is written so as to be equal to zero for a spin state $S_i = -1$ (i.e., for LS sites) and nonzero for the HS
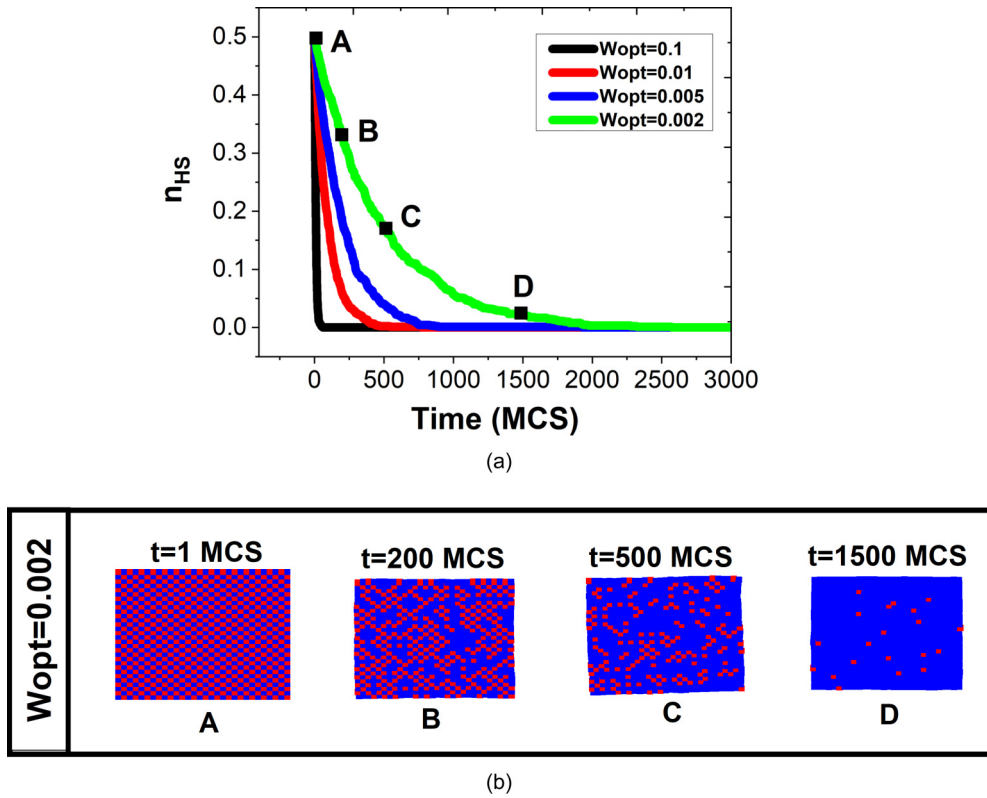
(a)

(b)

FIG. 9. (a) Time dependence (MCS) of the HS fraction during the reverse-LIESST process from HS-LS to LS-LS states at 10 K, for different W^{opt} values, showing the dependence of the transformation velocity on light intensity. (b) Selected snapshots of the spin configuration along the photoexcitation process for $W^{opt} = 0.002$ showing evidence of the random process transformation.

site. Assuming that the conversion of the HS sites follows an exponential behavior with the light excitation, then we have

$$W^{opt}(S_i \to -S_i) = \sigma(1 - S_i), \qquad (9)$$

where σ corresponds to the average quantum yield of the HS to LS photoexcitation process, which depends on the optical absorption of a photon by a molecule, the intensity of light and the Franck-Condon transition rates [66]. This factor defines the effective probability per unit time of optical switching HS $\to$ LS when the molecule is under light irradiation.

1. High-spin to low-spin photoexcitation

To mimic the experimental reverse-LIESST, where we generate the hidden stable LS-LS state from the intermediate HS-LS state as explained in Sec. III (experimental part), the same procedure is followed in this section where we initially prepare the system in the antiferromagnetic intermediate configuration at fixed temperature $T = 10$ K. The photoexcitation from this state is studied for different light intensities, as depicted in Fig. 9(a), which shows that for low-intensity value ($W^{opt} = 0.002$), the complete switching of the system to the pure LS state takes place after 2000 MCS. Increasing the value of the intensity decreases the conversion time as expected. It is remarked that the behavior of all curves follows an exponential behavior which denotes a noncooperative or random transformation process. Indeed, the snapshots B and C of Fig. 9(b) clearly show the appearance of disorder during transformation process (uncorrelated transformation).

It is, however, important to notice that illumination at higher temperature will lead to a different behavior due to the role of temperature, as it will be proved in the next section.

2. Reverse-light-induced thermal hysteresis by MC simulations

This section is devoted to the study of the reverse-LITH which consists in a competition between the light and temperature processes. In the experimental study of the reverse-LITH, we evidenced the stability of the LS-LS state by obtaining a first-order transition with domain propagation from this ground state to the intermediate HS-LS state on heating. To reproduce theoretically this behavior, we first prepare the system in the intermediate antiferromagnetic state at $T = 110$ K, we then cool down until $T = 40$ K, and warm up under light until $T = 110$ K, using the modified transition probabilities of Eq. (9). The obtained results of these simulations are represented in Fig. 10(a) which shows the occurrence of a light-induced thermal hysteresis loop in good qualitative agreement with the experimental data of Fig. 6(a). From the fundamental point of view, this hysteresis expresses the presence a bistability resulting from the competition between the noncooperative light process which favors the emergence of the LS state and the cooperative thermal relaxation. On cooling from the intermediate state, light and temperature play on the same way by stabilizing the LS state, while on heating from the LS state, the temperature stabilizes the intermediate state and the light tries to keep the system in the LS state. The hysteresis is then caused by the antagonist effects of light
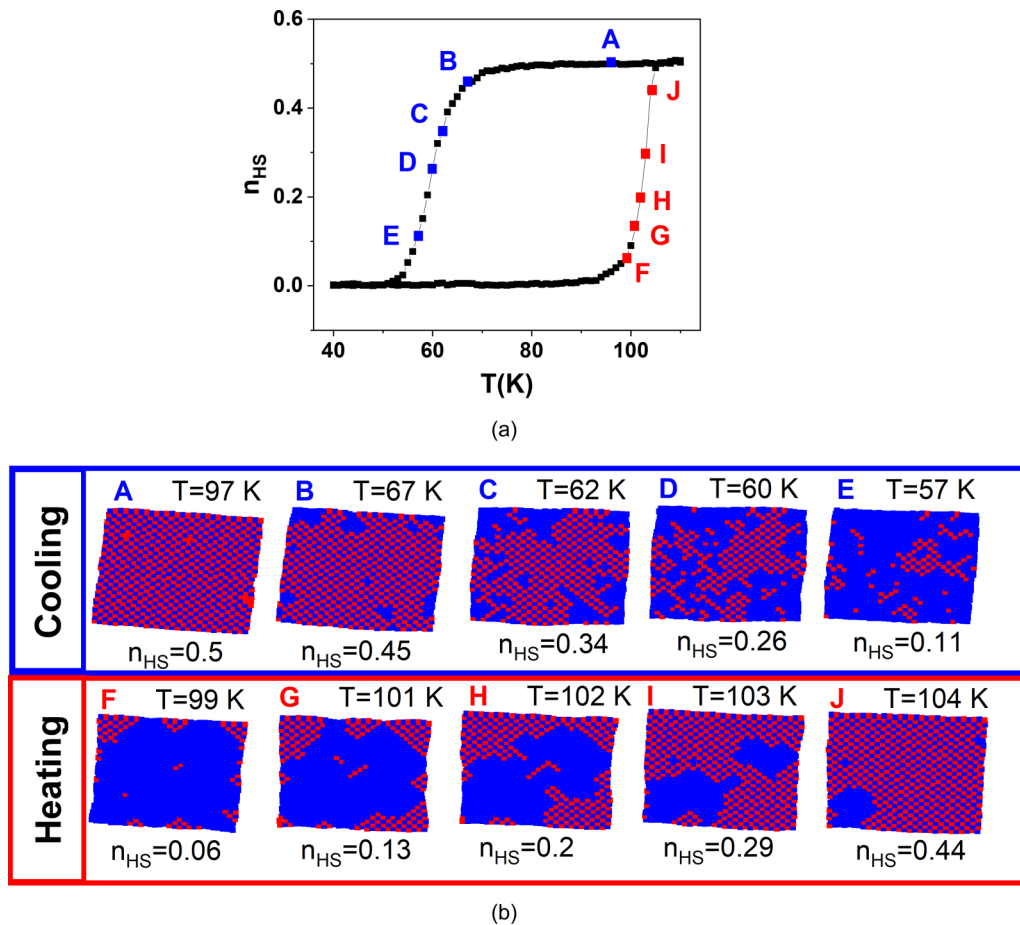
FIG. 10. (a) Reverse-LITH of the HS fraction, n_{HS}, obtained by MC simulations under a permanent irradiation for $W^{opt} = 2 \times 10^{-3}$ (a.u). The simulations are done by cooling from the antiferromagnetic metastable configuration at $n_{HS} = 0.5$ at $T = 110$ K until 40 K and then heating back. (b) Selected snapshots showing the spin organization along the process. Red and blue dots correspond to HS and LS sites. All other parameters are the same as those of Fig. 8.

and temperature which result in an instability of the high-spin fraction.

To get more insights about the spatiotemporal process of the system under light, we display in Fig. 10(b) some selected snapshots (A–E) of the spin-state organization on cooling, from the intermediate state, showing a similar behavior as that of photoexcitation process with an almost homogeneous transformation. Indeed, the LS domains appear from everywhere in the lattice including the center, thus confirming the noncooperative character of this transition (nonequilibrium process) which takes place around 60 K in a large temperature interval (~20 K). In contrast, on heating from the LS-LS state, the transformation is sharper and takes place in only few temperature steps (less than 5 K) between the LS-LS state and the intermediate state HS-LS [E and F snapshots in Fig. 10(b)]. Here, macroscopic HS-LS domains appear from the corners and propagate along the center of the lattice, which is the strong signature of the occurrence of a true first-order transition on heating between two thermodynamic stable states. Overall, these results demonstrate the stability of the LS-LS state and then the existence of a hidden state at low temperature accessible by photoexcitation. Crystallographic investigations performed on the homologous compound [50] Fe(2-pytrz)$_2$[Pt(CN)$_4$]}].3H$_2$O (where Pd is replaced by Pt)

allowed to identify that the strong metastability of the intermediate HS-LS state originates from the existence of a strong elastic frustration causing antiferroelastic interactions within the [FePt(CN)$_4$] layers, through the rigid NC-Pt-CN bridges connecting inequivalent Fe(II) sites.

V. CONCLUSION

In this work, we provided an OM investigation of photoinduced effects on SCO single crystal, exhibiting an incomplete first-order spin transition between a fully HS-HS state and an intermediate HS-LS state. We visualized by OM the photoswitching of the single crystal under irradiation by near-infrared light ($\lambda = 790$ nm). We found that the photoexcitation converts the HS-LS phase to LS-LS in a homogeneous way by changing the average optical density from that of HS-LS state to that of LS-LS state. The thermal relaxation of the obtained LS-LS state to the intermediate HS-LS in the dark is also monitored by OM, which revealed the existence of nucleation and single-domain propagation, proving the first-order character of this phase transformation. Next, we performed the reverse-LITH study where we visualized along the cooling branch a homogeneous transformation, while on heating from the LS-LS state to the intermediate HS-LS,

the transformation showed again a single-domain propagation behavior. The results confirm the thermodynamic first-order character of the transition from LS-LS to HS-LS state, which strengthens the idea that the LS-LS state (accessible by light) is a hidden stable state.

To reproduce theoretically these observations, we performed MC simulations on a 2D square lattice using an adapted version of the electroelastic model accounting for the existence of two nonequivalent sites in the lattice, having two different ligand fields. The elastic constants have been taken independent on the spin states and equal for the two types of sites. The model is first solved to investigate the thermal behaviors of the HS fraction and the average lattice parameter by monitoring the NN elastic constant value. Two-step transitions have been found, but the plateau at the transition was found to vanish with increasing the elastic constant. Thus, an elastic frustration introducing antagonist NN and NNN lattice spacing in the LS and HL state allowed to reproduce incomplete spin transition with a plateau at $n_{HS} = 0.5$ and a hidden LS-LS state. In a similar way as for the experimental investigations, we introduced the light effect in the MC procedure through the introduction of a bias in the Metropolis transition rates. This allowed to study the reverse-LIESST effect between the intermediate HS-LS and LS-LS states by MC simulation, which evidenced a homogeneous transformation. In contrast, the meticulous examination of the reverse-LITH revealed the first-order character of the transition from LS-LS to HS-LS state and so the stability of the LS-LS state at low temperature.

[1] P. Gütlich and H. Goodwin, Spin crossover: An overall perspective, in *Spin Crossover in Transition Metal Compounds I*, Topics in Current Chemistry (Springer, Berlin, 2004), Vol. 233, pp. 1–47.

[2] P. Gütlich, A. Hauser, and H. Spiering, Thermal and optical switching of iron(II) complexes, Angew. Chem. Int. Ed. Engl. **33**, 2024 (1994).

[3] E. König, in *Complex Chemistry*, Structure and Bonding (Springer, Berlin, 1991), pp. 51–152.

[4] E. Coronado, Molecular magnetism: from chemical design to spin control in molecules, materials and devices, Nat. Rev. Mater. **5**, 87 (2020).

[5] K. Boukheddaden, M. H. Ritti, G. Bouchez, M. Sy, M. M. Dîrtu, M. Parlier, J. Linares, and Y. Garcia, Quantitative contact pressure sensor based on spin crossover mechanism for civil security applications, J. Phys. Chem. C **122**, 7597 (2018).

[6] J. Linares, E. Codjovi, and Y. Garcia, Pressure and temperature spin crossover sensors with optical detection, Sensors **12**, 4479 (2012).

[7] P. Gütlich, Y. Garcia, and H. A. Goodwin, Spin crossover phenomena in Fe(II) complexes, Chem. Soc. Rev. **29**, 419 (2000).

[8] H. A. Goodwin, Spin crossover in cobalt(II) systems, in *Spin Crossover in Transition Metal Compounds II*, edited by P. Gütlich and H. Goodwin, Topics in Current Chemistry (Springer, Berlin, 2004), pp. 23–47.

[9] Y. Garcia and P. Gütlich, Thermal spin crossover in Mn(II), Mn(III), Cr(II) and Co(III) coordination compounds, in *Spin Crossover in Transition Metal Compounds II*, edited by P. Gütlich and H. Goodwin, Topics in Current Chemistry (Springer, Berlin, 2004), pp. 49–62.

[10] A. Bousseksou, N. Negre, M. Goiran, L. Salmon, J. P. Tuchagues, M. L. Boillot, K. Boukheddaden, and F. Varret, Dynamic triggering of a spin-transition by a pulsed magnetic field, Eur. Phys. J. B **13**, 451 (2000).

[11] A. Hauser, J. Jeftic, H. Romstedt, R. Hinek, and H. Spiering, Cooperative phenomena and light-induced bistability in iron(II) spin-crossover compounds, Coord. Chem. Rev. **190-192**, 471 (1999).

[12] S. Pillet, J. Hubsch, and C. Lecomte, Single crystal diffraction analysis of the thermal spin conversion in [Fe(btr)$_2$(NCS)$_2$](H$_2$O): Evidence for spin-like domain formation, Eur. Phys. J. B **38**, 541 (2004).

[13] S. Gawali-Salunke, F. Varret, I. Maurin, C. Enachescu, M. Malarova, K. Boukheddaden, E. Codjovi, H. Tokoro, S. Ohkoshi, and K. Hashimoto, Magnetic and mössbauer investigation of the photomagnetic prussian blue analogue Na$_{0.32}$Co[Fe(CN)$_6$]$_{0.74}$·3.4H$_2$O: Cooperative relaxation of the thermally quenched state, J. Phys. Chem. B **109**, 8251 (2005).

[14] F. Varret, C. Chong, A. Goujon, and K. Boukheddaden, Light-induced phase separation (LIPS) in [Fe(ptz)$_6$](BF$_4$)$_2$ spin-crossover single crystals: Experimental data revisited through optical microscope investigation, J. Phys.: Conf. Ser. **148**, 012036 (2009).

[15] C. Chong, A. Slimani, F. Varret, K. Boukheddaden, E. Collet, J. C. Ameline, R. Bronisz, and A. Hauser, The kinetics features of a thermal spin transition characterized by optical microscopy on the example of [Fe(bbtr)$_3$](ClO$_4$)$_2$ single crystals: Size effect and mechanical instability, Chem. Phys. Lett. **504**, 29 (2011).

[16] A. Goujon, F. Varret, K. Boukheddaden, C. Chong, J. Jeftic, Y. Garcia, A. D. Naik, J. C. Ameline, and E. Collet, An optical microscope study of photo-switching and relaxation in single crystals of the spin transition solid [Fe(ptz)$_6$](BF$_4$)$_2$, with image processing, Inorg. Chim. Acta **361**, 4055 (2008).

[17] C. Chong, H. Mishra, K. Boukheddaden, S. Denise, G. Bouchez, E. Collet, J.-C. Ameline, A. D. Naik, Y. Garcia, and F. Varret, Electronic and structural aspects of spin transitions observed by optical microscopy. the case of [Fe(ptz)$_6$](BF$_4$)$_2$, J. Phys. Chem. B **114**, 1975 (2010).

[18] A. Slimani, F. Varret, K. Boukheddaden, C. Chong, H. Mishra, J. Haasnoot, and S. Pillet, Visualization and quantitative analysis of spatiotemporal behavior in a first-order thermal spin transition: A stress-driven multiscale process, Phys. Rev. B **84**, 094442 (2011).

[19] F. Varret, A. Slimani, K. Boukheddaden, C. Chong, H. Mishra, E. Collet, J. Haasnoot, and S. Pillet, The propagation of the

thermal spin transition of $[Fe(btr)_2(NCS)_2](H_2O)$ single crystals, observed by optical microscopy, New J. Chem. **35**, 2333 (2011).

[20] M. Sy, F. Varret, K. Boukheddaden, G. Bouchez, J. Marrot, S. Kawata, and S. Kaizaki, Structure-driven orientation of the high-spin–low-spin interface in a spin-crossover single crystal, Angew. Chem. **126**, 7669 (2014).

[21] H. Fourati, E. Milin, A. Slimani, G. Chastanet, Y. Abid, S. Triki, and K. Boukheddaden, Interplay between a crystal's shape and spatiotemporal dynamics in a spin transition material, Phys. Chem. Chem. Phys. **20**, 10142 (2018).

[22] H. Fourati, G. Bouchez, M. Paez-Espejo, S. Triki, and K. Boukheddaden, Spatio-temporal investigations of the incomplete spin transition in a single crystal of $[Fe(2\text{-}pytrz)_2Pt(CN)_4]\cdot 3H_2O$: Experiment and theory, Crystals **9**, 46 (2019).

[23] M. Sy, R. Traiche, H. Fourati, Y. Singh, F. Varret, and K. Boukheddaden, Spatiotemporal investigations on light-driven high-spin–low-spin interface dynamics in the thermal hysteresis region of a spin-crossover single crystal, J. Phys. Chem. C **122**, 20952 (2018).

[24] F. Varret, C. Chong, A. Slimani, D. Garrot, Y. Garcia, and A. D. Naik, Real-time observation of spin-transitions by optical microscopy, in *Spin-Crossover Materials* (Wiley, Hoboken, NJ, 2013), p. 425.

[25] S. Bedoui, G. Molnár, S. Bonnet, C. Quintero, H. J. Shepherd, W. Nicolazzi, L. Salmon, and A. Bousseksou, Raman spectroscopic and optical imaging of high spin/low spin domains in a spin crossover complex, Chem. Phys. Lett. **499**, 94 (2010).

[26] J. Sanchez Costa, Macroscopic methods: Magnetic, optical, and calorimetric techniques, C. R. Chimie **21**, 1121 (2018).

[27] K. Ridier, G. Molnár, L. Salmon, W. Nicolazzi, and A. Bousseksou, Hysteresis, nucleation and growth phenomena in spin-crossover solids, Solid State Sci. **74**, A1 (2017).

[28] K. Nishi, S. Arata, N. Matsumoto, S. Iijima, Y. Sunatsuki, H. Ishida, and M. Kojima, One-dimensional spin-crossover iron(ii) complexes bridged by intermolecular imidazole−pyridine NH···N hydrogen bonds, $[Fe(HLMe)_3]X_2$ (HLMe = (2-methylimidazol-4-yl-methylideneamino-2-ethylpyridine; X = PF_6, ClO_4, BF_4), Inorg. Chem. **49**, 1517 (2010).

[29] M. Koike, K. Murakami, T. Fujinami, K. Nishi, N. Matsumoto, and Y. Sunatsuki, Syntheses, three types of hydrogen-bonded assembly structures, and magnetic properties of $[Fe^{III}(Him)_2(hapen)]Y\cdot solvent$ (Him = imidazole, hapen = N, N′-bis(2-hydroxyacetophenylidene)ethylenediamine, Y = BPh_4^-, $CF_3SO_3^-$, PF_6^-, ClO_4^-, and BF_4^-), Inorg. Chim. Acta **399**, 185 (2013).

[30] M. Paez-Espejo, M. Sy, F. Varret, and K. Boukheddaden, Quantitative macroscopic treatment of the spatiotemporal properties of spin crossover solids based on a reaction diffusion equation, Phys. Rev. B **89**, 024306 (2014).

[31] J. Wajnflasz and R. Pick, Transition low spin high spin dans les complexes de Fe^{2+}, Le J. Phys. Colloq. **32**, C1-91 (1971).

[32] A.-I. Popa, L. Stoleriu, and C. Enachescu, Tutorial on the elastic theory of spin crossover materials, J. Appl. Phys. **129**, 131101 (2021).

[33] W. Nicolazzi, S. Pillet, and C. Lecomte, Photoinduced phase separation in spin-crossover materials: Numerical simulation of a dynamic photocrystallographic experiment, Phys. Rev. B **80**, 132102 (2009).

[34] M. Sy, D. Garrot, A. Slimani, M. Paez-Espejo, F. Varret, and K. Boukheddaden, Reversible control by light of the high-spin low-spin elastic interface inside the bistable region of a robust spin-transition single crystal, Angew. Chem. Int. Ed. **55**, 1755 (2016).

[35] R. Traiche, M. Sy, H. Oubouchou, G. Bouchez, F. Varret, and K. Boukheddaden, Spatiotemporal observation and modeling of remarkable temperature scan rate effects on the thermal hysteresis in a spin-crossover single crystal, J. Phys. Chem. C **121**, 11700 (2017).

[36] A. Slimani, F. Varret, K. Boukheddaden, D. Garrot, H. Oubouchou, and S. Kaizaki, Velocity of the High-Spin Low-Spin Interface Inside the Thermal Hysteresis Loop of a Spin-Crossover Crystal, via Photothermal Control of the Interface Motion, Phys. Rev. Lett. **110**, 087208 (2013).

[37] S. Decurtins, P. Gütlich, C. P. Köhler, H. Spiering, and A. Hauser, Light-induced excited spin state trapping in a transition-metal complex: The hexa-1-propyltetrazole-iron (II) tetrafluoroborate spin-crossover system, Chem. Phys. Lett. **105**, 1 (1984).

[38] S. Decurtins, P. Gütlich, K. M. Hasselbach, A. Hauser, and H. Spiering, Light-induced excited-spin-state trapping in iron(II) spin-crossover systems, optical spectroscopic and magnetic susceptibility study, Inorg. Chem. **24**, 2174 (1985).

[39] A. Hauser, Intersystem crossing in the $[Fe(ptz)_6](BF_4)_2$ spin crossover system (ptz = 1-propyltetrazole), J. Chem. Phys. **94**, 2741 (1991).

[40] K. Boukheddaden and M. Sy, Direct optical microscopy observation of photo-induced effects and thermal relaxation in a spin crossover single crystal, Current Inorg. Chem. **6**, 40 (2016).

[41] A. Hauser, Intersystem crossing in Fe(II) coordination compounds, Coord. Chem. Rev. **111**, 275 (1991).

[42] E. Buhks, G. Navon, M. Bixon, and J. Jortner, Spin conversion processes in solutions, J. Am. Chem. Soc. **102**, 2918 (1980).

[43] Y. Ogawa, T. Ishikawa, S. Koshihara, K. Boukheddaden, and F. Varret, Effect of the magnetic field on the dynamics of the cooperative photoinduced spin-state transition and relaxation, Phys. Rev. B **66**, 073104 (2002).

[44] J. F. Letard, P. Guionneau, L. Rabardel, J. A. Howard, A. E. Goeta, D. Chasseau, and O. Kahn, Structural, magnetic, and photomagnetic studies of a mononuclear iron(II) derivative exhibiting an exceptionally abrupt spin transition. light-induced thermal hysteresis phenomenon, Inorg. Chem. **37**, 4432 (1998).

[45] A. Desaix, O. Roubeau, J. Jeftic, J. Haasnoot, K. Boukheddaden, E. Codjovi, J. Linarès, M. Noguès, and F. Varret, Light-induced bistability in spin transition solids leading to thermal and optical hysteresis, Eur. Phys. J. B **6**, 183 (1998).

[46] T. Delgado, A. Tissot, L. Guénée, A. Hauser, F. J. Valverde-Muñoz, M. Seredyuk, J. A. Real, S. Pillet, E.-E. Bendeif, and C. Besnard, Very long-lived photogenerated high-spin phase of a multistable spin-crossover molecular material, J. Am. Chem. Soc. **140**, 12870 (2018).

[47] S. Rat, J. S. Costa, S. Bedoui, W. Nicolazzi, G. Molnár, L. Salmon, and A. Bousseksou, Investigation of nucleation and growth phenomena during the thermal and light induced spin transition in the $[Fe(1\text{-}bpp)_2][BF_4]_2$ complex, Pure Appl. Chem. **87**, 261 (2015).

[48] K. Boukheddaden, H. Fourati, Y. Singh, and G. Chastanet, Evidence of photo-thermal effects on the first-order thermo-

induced spin transition of [{Fe(NCSe)(py)$_2$}$_2$(m-bpypz)] spin-crossover material, Magnetochemistry **5**, 21 (2019).

[49] R. H. Wiley and A. J. Hart, Reaction of diformylhydrazine with aminoheterocycles, J. Org. Chem. **18**, 1368 (1953).

[50] E. Milin, V. Patinec, S. Triki, E.-E. Bendeif, S. Pillet, M. Marchivie, G. Chastanet, and K. Boukheddaden, Elastic frustration triggering photoinduced hidden hysteresis and multistability in a two-dimensional photoswitchable Hofmann-like spin-crossover metal organic framework, Inorg. Chem. **55**, 11652 (2016).

[51] K. Boukheddaden, M. Sy, M. Paez-Espejo, A. Slimani, and F. Varret, Dynamical control of the spin transition inside the thermal hysteresis loop of a spin-crossover single crystal, Phys. B (Amsterdam) **486**, 187 (2016).

[52] See Supplemental Material at http://link.aps.org/supplemental/10.1103/PhysRevB.105.174436 for optical microscopy movies of the spatiotemporal transformation during (i) the reverse-LIESST photoexcitation process from HS-LS to LS-LS states, (ii) the thermal relaxation in the dark from LS-LS to the intermediate HS-LS state, (iii) the reverse-LITH loop between HS-LS and LS-LS states on cooling, as well as (iv) on heating from LS-LS to HS-LS during the reverse-LITH process showing the presence of a nucleation and domain growth.

[53] K. Boukheddaden, M. Sy, and F. Varret, Emergence of dynamical dissipative structures in a bistable spin crossover solid under light: Experience and theory, Adv. Theory Simul. **1**, 1800080 (2018).

[54] F. Varret, K. Boukheddaden, A. Goujon, B. Gillon, and G. J. McIntyre, Light-induced phase separation (LIPS) into like-spin phases observed by laue neutron diffraction on a single crystal of [Fe(*ptz*)$_6$](BF$_4$)$_2$, Z. Kristallogr. **223**, 250 (2008).

[55] F. Varret, K. Boukheddaden, C. Chong, A. Goujon, B. Gillon, J. Jeftic, and A. Hauser, Light-induced phase separation in the [Fe(*ptz*)$_6$](BF$_4$)$_2$ spin-crossover single crystal, Europhys. Lett. **77**, 30007 (2007).

[56] C. Chong, F. Varret, and K. Boukheddaden, Evolution of self-organized spin domains under light in single-crystalline [Fe(ptz)$_6$](BF$_4$)$_2$, Phys. Rev. B **81**, 014104 (2010).

[57] M. Ndiaye, Y. Singh, H. Fourati, M. Sy, B. Lo, and K. Boukheddaden, Isomorphism between the electro-elastic modeling of the spin transition and ising-like model with competing interactions: Elastic generation of self-organized spin states, J. Appl. Phys. **129**, 153901 (2021).

[58] G. D'Avino, A. Painelli, and K. Boukheddaden, Vibronic model for spin crossover complexes, Phys. Rev. B **84**, 104119 (2011).

[59] S. W. Biernacki and B. Clerjaud, Thermally driven low-spin high-spin phase transitions in solids, Phys. Rev. B **72**, 024406 (2005).

[60] K. Boukheddaden, I. Shteto, B. Hôo, and F. Varret, Dynamical model for spin-crossover solids. I. Relaxation effects in the mean-field approach, Phys. Rev. B **62**, 14796 (2000).

[61] A. C. Felts, A. Slimani, J. M. Cain, M. J. Andrus, A. R. Ahir, K. A. Abboud, M. W. Meisel, K. Boukheddaden, and D. R. Talham, Control of the speed of a light-induced spin transition through mesoscale core–shell architecture, J. Am. Chem. Soc. **140**, 5814 (2018).

[62] M. Paez-Espejo, M. Sy, and K. Boukheddaden, Elastic frustration causing two-step and multistep transitions in spin-crossover solids: Emergence of complex antiferroelastic structures, J. Am. Chem. Soc. **138**, 3202 (2016).

[63] M. Paez-Espejo, M. Sy, and K. Boukheddaden, Unprecedented bistability in spin-crossover solids based on the retroaction of the high spin low-spin interface with the crystal bending, J. Am. Chem. Soc. **140**, 11954 (2018).

[64] A. Slimani and K. Boukheddaden, An electro-elastic theory for the mechanically-assisted photo-induced spin transition in core–shell spin-crossover nanoparticles, Phys. Chem. Chem. Phys. **20**, 28583 (2018).

[65] C. Enachescu, L. Stoleriu, M. Nishino, S. Miyashita, A. Stancu, M. Lorenc, R. Bertoni, H. Cailleau, and E. Collet, Theoretical approach for elastically driven cooperative switching of spin-crossover compounds impacted by an ultrashort laser pulse, Phys. Rev. B **95**, 224107 (2017).

[66] A. Slimani, K. Boukheddaden, F. Varret, M. Nishino, and S. Miyashita, Properties of the low-spin high-spin interface during the relaxation of spin-crossover materials, investigated through an electro-elastic model, J. Chem. Phys. **139**, 194706 (2013).